

# Synthesis of nanocrystals and morphology control of hydrothermally prepared $\text{LiFePO}_4$ †‡

B. Ellis, Wang Hay Kan, W. R. M. Makahnouk and L. F. Nazar\*

Received 10th April 2007, Accepted 25th May 2007

First published as an Advance Article on the web 12th June 2007

DOI: 10.1039/b705443m

Lithium transition metal phosphate olivines such as  $\text{LiFePO}_4$  have been recognized as very promising electrodes for lithium-ion batteries because of their energy storage capacity combined with electrochemical and thermal stability. A key issue in these materials is to determine the synthetic conditions for optimum control of particle size and morphology, and ideally to find those that result in nanocrystalline products. Here, we report a full study that examines the synthesis of the material *via* hydrothermal methods to give single phase nanocrystalline materials for  $\text{LiFePO}_4$  and  $\text{LiMnPO}_4$ , and their solid solutions with  $\text{Mg}^{2+}$ . A reaction mechanism is proposed. Variation of the synthesis parameters showed that increasing reactant concentration strongly favours the formation of nanocrystalline products, but as less defect-free materials are formed at temperatures above 180 °C, and ideally above 200 °C, control of nucleation and growth can (and should) also be effected using polymeric or surfactant additives. The nature of the precursor and carbon-containing additives in the autoclave also have profound effects on morphology and the electrochemical properties.

## Introduction

Hydrothermal (HDT) chemistry is one of the principal synthetic methods for the preparation of new inorganic materials. It is used to produce various nanomaterials such as zeolites,<sup>1</sup> oxides<sup>2</sup> and phosphates<sup>3</sup> which are functional in catalysis, electrochemistry and separation science. These compounds may have intriguing morphologies such as nanospheres,<sup>4</sup> nanowires<sup>5</sup> and nanotubes.<sup>6</sup> Control of the products comes as a result of careful manipulation of concentration, pH and temperature.

Nanomaterials are of significant importance to the field of lithium battery materials. Electrode nanomaterials offer the potential for high electrode/electrolyte surface contact, lesser mechanical strain upon lithium (de)intercalation from the lattice and reduced path lengths for lithium-ion/electron transport through the material which can lead to high rate capability. In previous reports, hydrothermal synthesis has been utilized to produce lithium iron phosphate,<sup>7–9</sup> an increasingly popular electrode material for lithium ion batteries as a result of its promising electrochemical properties and low toxicity. It adopts the olivine structure (*Pnma*), with lithium nestled in the M1 sites to form linear chains of edge-sharing octahedra along the direction of the *b*-axis. The iron cations occupy the M2 sites, to generate planes of corner-shared octahedra in the *bc* plane.<sup>10</sup> These chains are bridged by edge and corner shared phosphate tetrahedra, to create a rigid

three-dimensional structure as shown in Fig. 1a. One of the inherent difficulties in electrochemical cycling of this material is its low electronic conductivity ( $10^{-9} \text{ S cm}^{-1}$  at room temperature),<sup>11</sup> which prevents achievement of full theoretical capacity ( $170 \text{ mAh g}^{-1}$ ) at very high rates. Introducing varying amounts of carbon (1–15 wt%) into  $\text{LiFePO}_4$  improves the bulk conductivity and can have a beneficial effect on particle size.<sup>12,13</sup> More importantly, decreasing the size of the  $\text{LiFePO}_4$  crystallites to nanodimensions reduces the distance the lithium ions and electrons must be transported through the lattice, and may ease the strain associated with the two-phase redox

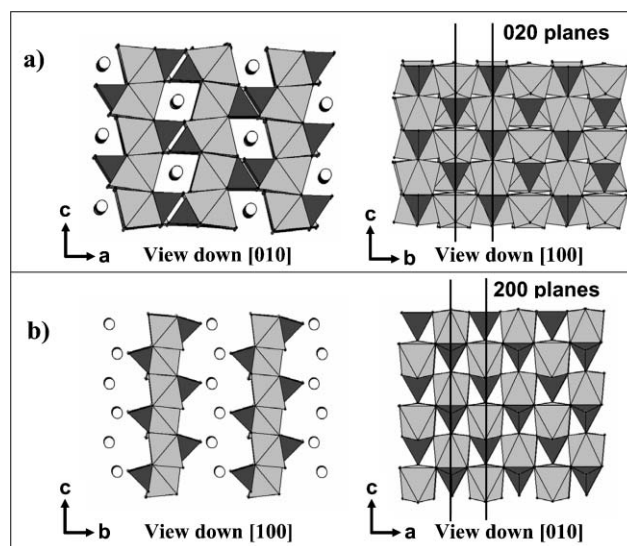


**Fig. 1** a) The olivine structure, adopted by several minerals including  $\text{LiFePO}_4$ , in the space group *Pnma*; b) structure of  $\text{NH}_4\text{FePO}_4 \cdot \text{H}_2\text{O}$  in the space group *Pmn2*<sub>1</sub> showing the comparison to the olivine structure.

University of Waterloo, Department of Chemistry, Waterloo, Ontario, Canada N2L 3G1

† This paper is part of a *Journal of Materials Chemistry* theme issue on New Energy Materials. Guest editor: M. Saiful Islam.

‡ Electronic supplementary information (ESI) available: XRD patterns of  $\text{LiMnPO}_4$ ,  $\text{Li}(\text{Mn}_{0.6}\text{Fe}_{0.4})\text{PO}_4$ ,  $\text{Li}(\text{Mn}_{0.4}\text{Fe}_{0.6})\text{PO}_4$  and  $\text{LiFePO}_4$ . See DOI: 10.1039/b705443m

reaction between  $\text{LiFePO}_4$  and  $\text{FePO}_4$ . These factors enhance electrode performance.<sup>14</sup>

Of the many synthetic methods reported for this material, hydrothermal synthesis is the most intriguing, owing to the low cost of precursors, comparatively short reaction times and the possibility for large scale batch reactions. Commercial production of  $\text{LiFePO}_4$  is under way by this process, in fact, although little is known about the methodology.<sup>15</sup> Previous seminal reports on this material have described iron and lithium disordering on the M1 and M2 sites for materials prepared at low temperatures ( $<130\text{ }^\circ\text{C}$ ), which contributes to a loss of capacity.<sup>8</sup> Subsequent work has shown that the disorder is minimized at higher temperatures.<sup>16,17</sup> This study explores *in-situ* hydrothermal synthesis of  $\text{LiFePO}_4$  directed towards understanding the mechanism of growth, and the morphology and crystallite size as a function of precursor, precursor concentration, pH and temperature. We have furthermore used organic reagents to control the morphology and carbon surface coverage of  $\text{LiFePO}_4$  nanomaterials.

## Experimental

### Synthesis

Carbon-free triphylite samples were prepared from  $(\text{NH}_4)_2\text{Fe}(\text{SO}_4)_2 \cdot 6\text{H}_2\text{O}$  (Alfa Aesar),  $\text{H}_3\text{PO}_4$  (Fisher) and  $\text{LiOH} \cdot \text{H}_2\text{O}$  (Alfa Aesar) in a 1 : 1 : 3 molar ratio. Carbon-containing samples were prepared from the same quantities and reagents as carbon-free materials with the addition of various organic additives (as described in the text), in the ratio of 1 : 1 : 3 : 0.25. For all syntheses, the reactants were stirred in a sealed 45 ml Parr autoclave at  $140\text{--}220\text{ }^\circ\text{C}$  for 0.5–24 hours. Subsequent sintering of the products took place at  $600\text{--}800\text{ }^\circ\text{C}$  under flowing Ar. In the case of using  $\text{NH}_4\text{FePO}_4 \cdot \text{H}_2\text{O}$  as the precursor in the autoclave, single-phase triphylite was prepared from  $\text{NH}_4\text{FePO}_4 \cdot \text{H}_2\text{O}$ ,  $\text{LiOH} \cdot \text{H}_2\text{O}$  (Alfa Aesar) and ascorbic acid in a 4 : 4 : 3 molar ratio, typically using a concentration of  $\text{NH}_4\text{FePO}_4 \cdot \text{H}_2\text{O}$  of 0.133 M. The reagents were placed in an autoclave which was heated at  $190\text{ }^\circ\text{C}$  for 15 hours. The product was filtered off and dried in a vacuum oven at  $60\text{ }^\circ\text{C}$  for 3 hours. Surfactants such as the block copolymer P123 [(EO)<sub>20</sub>, (PO)<sub>70</sub>, (EO)<sub>20</sub>]; BASF], and Jeffamine D230 [a polyoxyalkylamine, Sigma/Fluka] were also used as additives in selected reactions.

### XRD and SEM

X-Ray diffraction was performed on a Bruker D8-Advantage powder diffractometer using  $\text{Cu-K}\alpha$  radiation ( $\lambda = 1.5405\text{ \AA}$ ) from  $2\theta = 10$  to  $80$  degrees at a count rate of 1 s per step of  $0.02^\circ$ . X-Ray datasets were refined by conventional Rietveld methods using the GSAS package with the EXPGUI interface.<sup>18</sup> Background, scale factor, zero point, lattice parameters, atomic positions, and coefficients for the peak shape function were iteratively refined until convergence was achieved. SEM samples were gold coated and examined in a LEO 1530 field emission scanning electron microscope (FESEM) instrument equipped with an energy dispersive X-ray spectroscopy (EDX) attachment. Images were recorded at 15 kV with a secondary electron detector. The Raman spectra were recorded with a

Renishaw 1000 spectrometer using a He–Ne laser with the excitation wavelength of  $632.8\text{ nm}$  as the radiation source; 25% of the total power ( $40\text{ mW}$ ) was employed for the measurements.

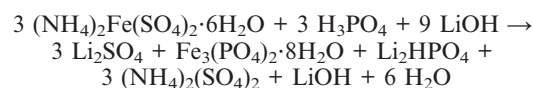
### Electrochemical measurements

Electrochemical evaluation of the materials was carried out in metallic lithium test coin cells using a commercial (MacPile<sup>TM</sup>) multichannel galvanostat/potentiostat operating in galvanostatic mode. Typical cathode loadings were in the range of  $5\text{--}6\text{ mg cm}^{-2}$  and an electrode diameter of  $10\text{ mm}$  was used throughout. The positive electrodes comprised 80 wt% active material, 10% Super S carbon and 10 wt% PVDF binder. The electrolyte was composed of a 1 M  $\text{LiPF}_6$  solution in 1 : 1 EC–DMC.

## Results and discussion

### a) Reaction mechanism

Addition of  $\text{LiOH}$  to a mixture of  $(\text{NH}_4)_2\text{Fe}(\text{SO}_4)_2 \cdot 6\text{H}_2\text{O}$  and  $\text{H}_3\text{PO}_4$  results in a basic solution ( $\text{pH} = 8.3$ ) and precipitation of an amorphous green-yellow solid. In contrast, crystalline green vivianite ( $\text{Fe}_3(\text{PO}_4)_2 \cdot 8\text{H}_2\text{O}$ ) is produced by the addition of  $\text{LiOH}$  to a similar solution containing ascorbic acid. In both cases, lithium sulfate is detected in the remaining solution. We conclude the initial reaction in the hydrothermal vessel (before heating) is:



Hydrothermal treatment of the basic mixture at  $190\text{ }^\circ\text{C}$  for 30 minutes produced an intermediate phase, formed as crystalline “nanoleaflets” detectable by X-ray diffraction (Fig. 2a,d). It exhibits a relatively weak and disordered XRD pattern, albeit with one very strong, characteristic reflection at

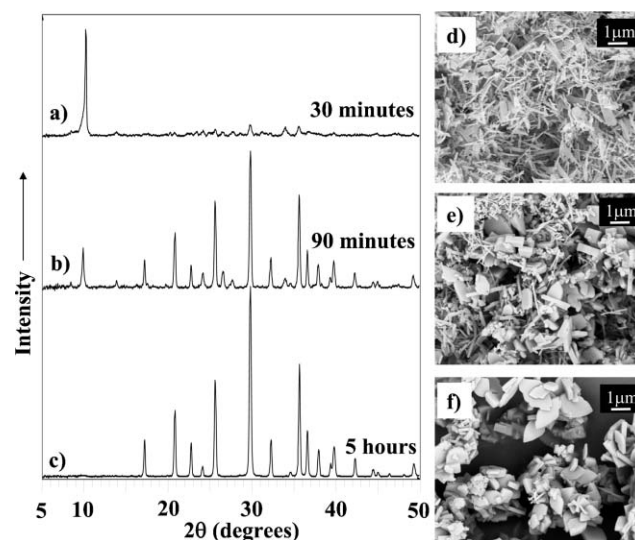


**Fig. 2** Powder X-ray diffraction patterns and corresponding SEM micrographs of hydrothermal  $\text{LiFePO}_4$  after various reaction times, depicting the presence of an intermediate that reacts to form  $\text{LiFePO}_4$ : 30 minutes (a, d), 90 minutes (b, e) and 5 hours (c, f).

$2\theta = 9.8^\circ$ . Elemental analysis of material extracted from the autoclave at this stage confirmed a lithium to iron ratio of approximately 1 :5, indicative of partial reaction of the initial vivianite with the compounds present in the autoclave. Further sintering of this intermediate at  $600^\circ\text{C}$  under Ar produced a mixture of triphylite and graffonite ( $\text{Fe}_3(\text{PO}_4)_2$ ), again indicating partial lithiation. If the hydrothermal reaction is allowed to continue for 90 minutes at the same temperature, consumption of the leaflets occurs. This produces larger crystallites (Fig. 2e), coinciding with the detection of triphylite (Fig. 2b) in the XRD pattern. The reaction is not at completion, as some leaflets remain in the hydrothermal product. After 5 hours, however, the leaflets fully react to produce larger crystallites (Fig. 2f) signaling the synthesis of  $\text{LiFePO}_4$  is complete, as seen by the pure olivine phase in the X-ray diffraction pattern (Fig. 2c).

The XRD pattern of the intermediate, and its morphology (Fig. 2d), suggested that it may be related to  $\text{NH}_4\text{FePO}_4\cdot\text{H}_2\text{O}$ , whose XRD pattern is also dominated by a very prominent high-intensity reflection at  $2\theta = 9.8^\circ$  (JCPDS #45-0424). This corresponds to the (010) reflection in the  $Pmn2_1$  space group, and the intensity is due to a high degree of preferred orientation arising from the thin plate morphology of this material.<sup>19</sup> Comparison of the structures of  $\text{LiFePO}_4$  (Fig. 1a) and  $\text{NH}_4\text{FePO}_4\cdot\text{H}_2\text{O}$  (Fig. 1b) indicates how they could be related by a simple transformation. The connectivity of the iron and phosphate polyhedra in the (100) plane of  $\text{LiFePO}_4$  is identical to that in the corresponding (101) plane of  $\text{NH}_4\text{FePO}_4\cdot\text{H}_2\text{O}$  (note the difference in the space groups switches the  $a$  and  $b$  axes); similarly, the  $d$ -spacing corresponding to the (020) reflection in  $\text{LiFePO}_4$  is almost the same as the (200) reflection for  $\text{NH}_4\text{FePO}_4\cdot\text{H}_2\text{O}$  since the repeating polyhedral motif is the same, as illustrated in Fig. 1. We propose that the precursors

initially precipitated in the autoclave (*i.e.*,  $\text{Fe}_3(\text{PO}_4)_2\cdot 8\text{H}_2\text{O}$  and other amorphous solids) react with excess  $\text{NH}_4^+$  in solution to first form the ammonium intercalated solid  $\text{NH}_4\text{FePO}_4\cdot\text{H}_2\text{O}$  (Fig. 1b). Upon rapid subsequent exchange of  $\text{NH}_4^+$  for  $\text{Li}^+$  in the autoclave solution, the adjacent sheets are “knitted” together by condensation of the  $\text{LiO}_6$  octahedra to crystallize  $\text{LiFePO}_4$ . The reaction intermediate that we see after 30 minutes of reaction in the autoclave is clearly not pure  $\text{NH}_4\text{FePO}_4\cdot\text{H}_2\text{O}$ , but a material that has already undergone partial  $\text{Li}^+$  exchange to give rise to a disordered material. This is evident from the elemental analysis, and from direct comparison of the XRD patterns of the intermediate, and  $\text{NH}_4\text{FePO}_4\cdot\text{H}_2\text{O}$  shown in Fig. 3a which show a similarity but not exact correspondence.

Further evidence suggesting that  $\text{NH}_4\text{FePO}_4\cdot\text{H}_2\text{O}$  may be a reaction intermediate comes from the fact that it can be directly used as a precursor in the autoclave. The hydrothermal reaction of solid  $\text{NH}_4\text{FePO}_4\cdot\text{H}_2\text{O}$ , LiOH and ascorbic acid readily produced single-phase  $\text{LiFePO}_4$  (Fig. 3b) with a unique tablet-shaped morphology (Fig. 3c). This is in contrast to the diamond-shaped crystallites that are usually formed by HDT (see below, and reference 7 or 20). Small crystallites with basal dimensions of about 200 nm, and 100 nm thick were formed. Increasing the total concentration of the precursors yielded even smaller nanocrystallites, with basal dimensions on the order of 50 nm (Fig. 3d). This provoked our studies on the effect of concentration and temperature on the morphology of  $\text{LiFePO}_4$  formed from conventional reagents, as described in the following.

### b) Factors controlling crystallite size

The size of the crystallites in the absence of organic additives is controlled predominantly by the reaction temperature and

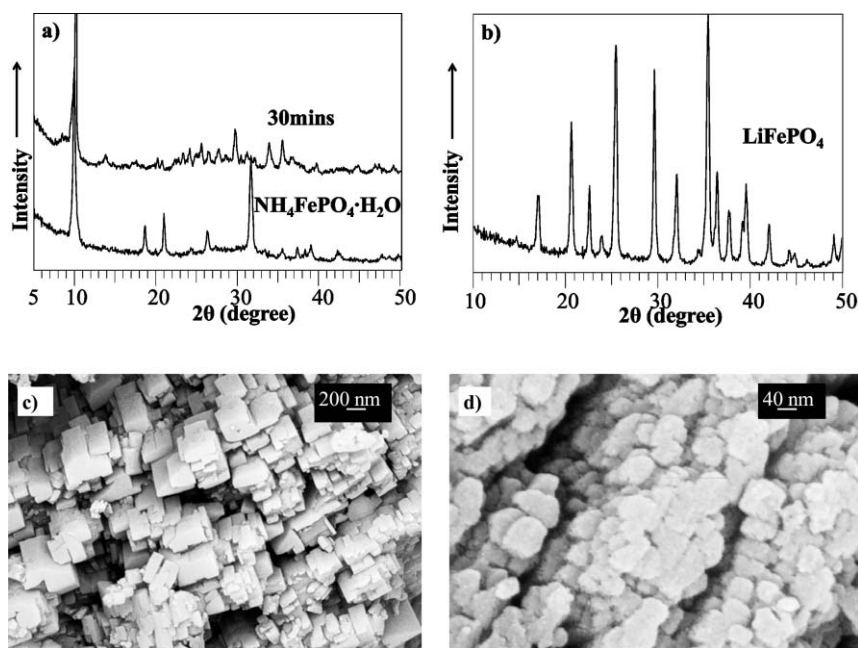


**Fig. 3** a) XRD pattern of the intermediate in the hydrothermal reaction after 30 minutes compared to the diffraction pattern of  $\text{NH}_4\text{FePO}_4\cdot\text{H}_2\text{O}$ ; b) XRD pattern of the single phase  $\text{LiFePO}_4$  that results from hydrothermal treatment of  $\text{NH}_4\text{FePO}_4\cdot\text{H}_2\text{O}$ ; c) SEM micrograph of the product shown in b); d) SEM micrograph of  $\text{LiFePO}_4$  produced from  $\text{NH}_4\text{FePO}_4\cdot\text{H}_2\text{O}$  at high concentrations.

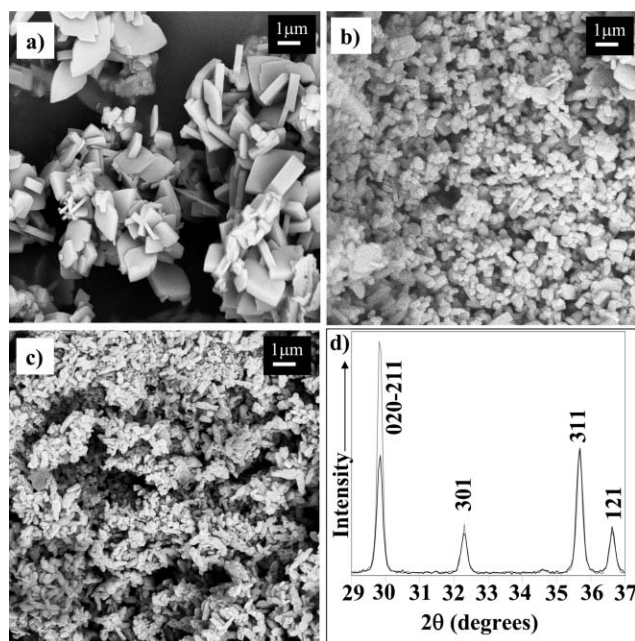


**Fig. 4** SEM micrographs of carbon-free  $\text{LiFePO}_4$  crystallized at different concentrations and temperatures: a) 0.25 M (Fe), 190 °C; b) 0.25 M (Fe), 140 °C; c) 0.75 M (Fe), 190 °C. Part (d) shows the XRD patterns of the compounds synthesized at 190 °C (0.25 M (Fe) in grey, 0.75 M (Fe) in black). Preferred orientation in the (020) direction is seen in the 0.25 M sample (grey). The (311) reflection has been normalized in the two patterns.

concentration of the precursors in the autoclave. At 190 °C, typical low concentrations of precursors (7 mmol of  $(\text{NH}_4)_2\text{Fe}(\text{SO}_4)_2 \cdot 6\text{H}_2\text{O}$  in 28 ml of water—or 0.25 M in Fe—along with stoichiometric amounts of  $\text{H}_3\text{PO}_4$   $\text{LiOH} \cdot \text{H}_2\text{O}$ ) produce diamond-shaped platelets that are about 250 nm thick. These have large basal dimensions of 1–5  $\mu\text{m}$  (Fig. 4a). Increasing the reactant concentration by threefold creates more nucleation sites and therefore produces much smaller particles, whose basal size distribution peaks at 250 nm (Fig. 4b). The corresponding XRD patterns are shown in Fig. 4d. The two patterns are normalized to the intensity of the most intense peak for triphylite, the (311) peak at 35.6°. While most of the peaks are of similar intensity, the peak at 29.8° is much more intense for the materials prepared using a lower concentration. As shown by Chen *et al.*,<sup>20</sup> the large diamond-shaped surfaces of hydrothermally prepared  $\text{LiFePO}_4$  correspond to the *ac* plane, which is perpendicular to the (020) direction. The increased intensity of the peak at 29.8° is the result of preferred orientation in the (020) direction. This is significant since this direction is the most facile pathway for lithium mobility in the material, as predicted by consideration of the structure, and as calculated by Morgan *et al.*<sup>21</sup> The large exposure of the electrochemically active crystal face represents approximately 80% of the surface area of each individual particle, and thus the thin profile of these particles reduces the lithium diffusion path length.

Although this prevailing morphology may show potential for improved electrochemistry, reducing the overall particle size of the electrode material is also important. As is the case with solid state or sol–gel techniques, this can be accomplished

by synthesis at lower temperatures. Material synthesized at 140 °C using an autoclave concentration of 0.25 M (Fe) produces substantially smaller particles than crystallites synthesized at 190 °C (Fig. 4c). The former temperature is the minimum to produce pure  $\text{LiFePO}_4$ . The heating period has little effect on the morphology of the hydrothermal product once the minimum reaction time (3 hours) is surpassed.

### c) Factors controlling crystallite purity

The purity of the products depends predominantly on the oxygen content of the gaseous headspace in the autoclave, and the oxidizing power of the medium. Trace impurity phases containing  $\text{Fe}^{3+}$  such as tavorite ( $\text{LiFePO}_4\text{OH}$ ), may be formed along with  $\text{LiFePO}_4$  if the atmosphere is too oxidizing. Tavorite is known to form under mild hydrothermal conditions. Upon subsequent heat treatment above 550 °C, it decomposes to  $\text{Li}_3\text{Fe}_2(\text{PO}_4)_3$  and  $\text{Fe}_2\text{O}_3$ .<sup>7</sup> Although these ferric compounds are formed in trace quantities in the reactor and are not readily detectable by X-ray diffraction,  $\text{Fe}_2\text{O}_3$  is clearly visible in a Raman spectrum of a sample fired at 600 °C under argon, along with the peaks characteristic of  $\text{LiFePO}_4$  (including the phosphate band at 960  $\text{cm}^{-1}$ , Fig. 5a).<sup>22</sup> These impurities are detrimental to the electrochemical performance of  $\text{LiFePO}_4$ , as shown in previous studies. They can be eliminated by purging oxygen from the solution and the headspace, giving rise to products that are free of  $\text{Fe}_2\text{O}_3$  and any other  $\text{Fe}^{3+}$  impurities (Fig. 5b) after heat treatment in Ar. However, although the materials are single-phase  $\text{LiFePO}_4$ , the electrochemical properties of these carbon-free samples are poor even if the particle size is small (<1  $\mu\text{m}$ ).

### d) Organic modifiers for carbon content and crystallite size

While the headspace of the autoclave is critical to producing single phase materials, organic molecules can be added to the bombs to act as internal reducing agents as seen in previous reports, such as ascorbic acid, sucrose and citric acid.<sup>20</sup> Citric acid and ascorbic acid have been utilized previously as carbon sources and reducing agents in various sol–gel and solid state methods to  $\text{LiFePO}_4$ .<sup>13,23</sup> Our motivation for adding organic

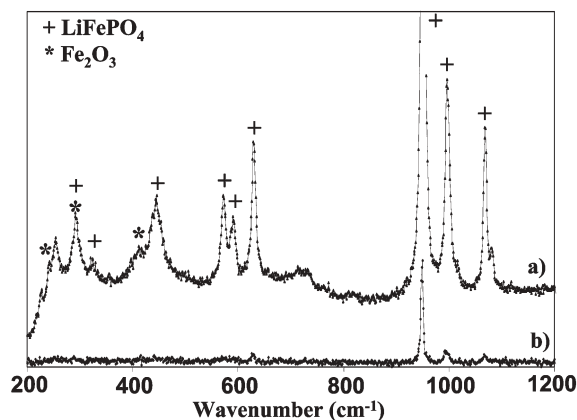


**Fig. 5** Raman spectra of carbon-free hydrothermal  $\text{LiFePO}_4$  fired at 600 °C under Ar after hydrothermal treatment: a) in the presence of air; and b) in an autoclave filled with nitrogen. The peaks of  $\text{LiFePO}_4$  and  $\text{Fe}_2\text{O}_3$  are labelled.

compounds to the autoclave prior to hydrothermal treatment is two-fold: firstly, it has been demonstrated previously that specific organic molecules control particle morphology. For example, ionic and non-ionic surfactants used in low-pressure hydrothermal reactions lead to the generation of mesoporous materials.<sup>24</sup> Secondly, subsequent heating of these organic compounds in inert atmospheres could decompose these compounds into carbonaceous films, depositing a thin conductive layer on the triphylite particles.

Products recovered from samples prepared at low concentration of precursors (0.25 M in Fe), containing ascorbic acid or citric acid heated at 190 °C and subsequently fired at 600 °C in flowing Ar, were all identified as pure LiFePO<sub>4</sub> by X-ray diffraction. Comparing the SEM images of these two samples (Fig. 6a and b) with those shown in Fig. 4 confirms that the presence of a reducing agent strongly affects the morphology. The particle size of the ascorbic acid sample is substantially smaller (250–1.5 μm) than without the reducing agent. Conversely, the sample with citric acid contains a wide distribution of particle sizes (500 nm–3 μm), with particle thicknesses considerably greater than those without additives. The morphology of this sample does not exhibit the monolithic sponge appearance of samples made with citric acid in the solid state.<sup>13</sup>

Raman spectroscopy was used to study the carbon microstructure. The Raman spectra show two important frequencies for carbon: 1350 cm<sup>-1</sup> corresponding to disorder in sp<sup>2</sup>-hybridized carbon (D-band) and 1590 cm<sup>-1</sup> corresponding to tangential stretching (E<sub>2g</sub>) in graphitic materials (G-band).<sup>25</sup> The Raman spectrum (Fig. 6c) identifies the deposition of significant quantities of carbon (approximately 5% wt) for the

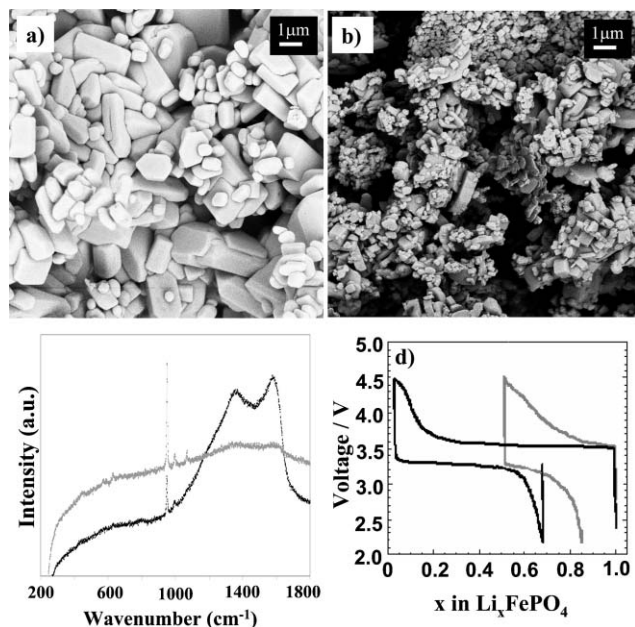


**Fig. 6** SEM images of hydrothermal LiFePO<sub>4</sub> treated with citric acid (a) and ascorbic acid (b) in the reactor. The corresponding Raman spectra and charge–discharge profiles are shown in (c) and (d) respectively, where the grey curves in both cases indicate the citric acid derived material, and the black curves refer to the ascorbic acid derived material.

ascorbic acid product. This is likely because ascorbic acid decomposes near 200 °C under typical conditions. The more stable citric acid does not decompose inside the hydrothermal reactor and as a result minimal carbon is detected. These discrepancies in particle size and carbon content are evident in a comparison of the electrochemistry of the two materials (Fig. 6d). With substantially more carbon and smaller average particle size, the ascorbic acid sample exhibits 70% reversibility on the first cycle, as opposed to 35% for the sample prepared from citric acid when cycled at a rate of C/10.

Nanoparticles of LiFePO<sub>4</sub> can be synthesized using water-soluble polymers such as polyacrylic acid as reducing agents. This polymer and the surfactants described below also act as strong coordinating agents that bind to the growing crystal faces, inhibiting growth and nucleation steps. Hydrothermal treatment with this additive produces 300–500 nm diameter agglomerated clusters consisting of very small particles that are 75–100 nm in size (Fig. 7b). Their diffraction pattern, together with a LeBail refinement is shown in Fig. 7a. The unit cell volume and *a* parameter are significantly smaller than those for typical hydrothermal or solid state LiFePO<sub>4</sub>, as summarized in Table 1. Although decreased unit cell volume for LiFePO<sub>4</sub> particles <100 nm in size has been reported earlier, without explanation,<sup>26,27</sup> change in lattice parameters of nano-powders as compared to bulk phases is a common phenomenon. The decrease in the lattice parameters of triphylite particles <100 nm is likely similar to that seen in other oxides of iron (γ-Fe<sub>2</sub>O<sub>3</sub>)<sup>28</sup> and cobalt (Co<sub>3</sub>O<sub>4</sub>).<sup>29</sup> In these cases, the decrease in lattice parameter was attributed to strain

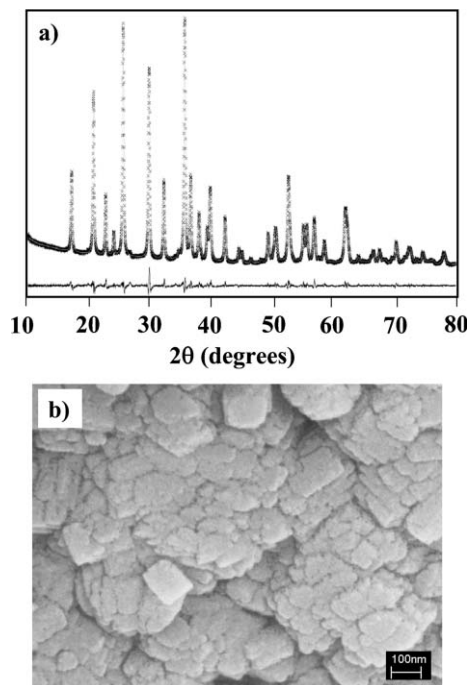


**Fig. 7** XRD pattern and LeBail (full pattern matching) refinement (a) and SEM micrograph (b) of LiFePO<sub>4</sub> synthesized hydrothermally in the presence of a water-soluble polymer, polyacrylic acid. The experimental (×) and calculated (—) diffraction patterns are shown, along with the difference curve. Lattice parameters and the agreement factor are given in Table 1.

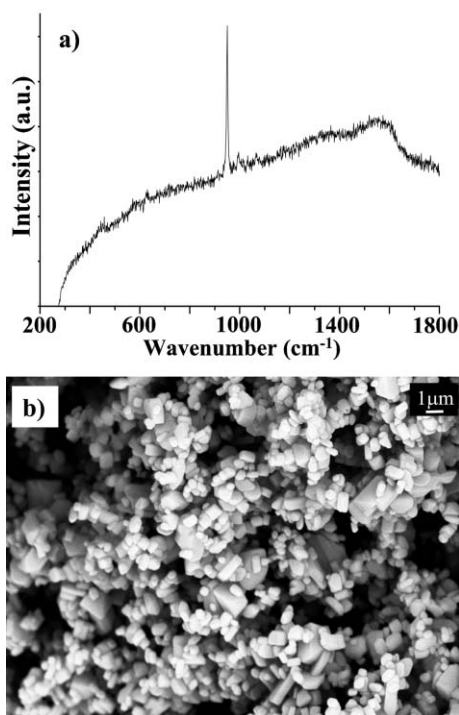
**Table 1** Comparison of lattice parameters for LiFePO<sub>4</sub> and LiMnPO<sub>4</sub>

LiFePO <sub>4</sub> synthetic route	Average crystallite size/nm	<i>a</i> /Å	<i>b</i> /Å	<i>c</i> /Å	<i>V</i> /Å <sup>3</sup>	<i>wR<sub>p</sub></i> (%)
Solid state	280	10.3222(2)	6.00566(8)	4.6941(1)	290.99	5.25
Hydrothermal	700	10.3328(2)	6.00296(5)	4.6950(1)	291.22	7.94
Nanocrystalline hydrothermal	100	10.3089(1)	5.9849(1)	4.6970(1)	289.79	6.65
LiMnPO <sub>4</sub> synthetic route	Average crystallite size/nm	<i>a</i> /Å	<i>b</i> /Å	<i>c</i> /Å	<i>V</i> /Å <sup>3</sup>	<i>wR<sub>p</sub></i> (%)
Solid state	300	10.4430(2)	6.1014(1)	4.7430(1)	302.22	6.12
Hydrothermal	550	10.4456(1)	6.09815(6)	4.7456(1)	302.29	5.61
Nanocrystalline hydrothermal	80	10.4476(1)	6.10225(7)	4.7485(1)	302.74	5.20

on the particles as a result of high surface tension. In contrast, cerium oxide, known to commonly undergo point defects in the bulk phase, undergoes an increase in lattice parameters.<sup>30</sup> The ramifications of this reduced lattice strain on the triphylite structure are under investigation.

### e) Surfactants to control crystallite size

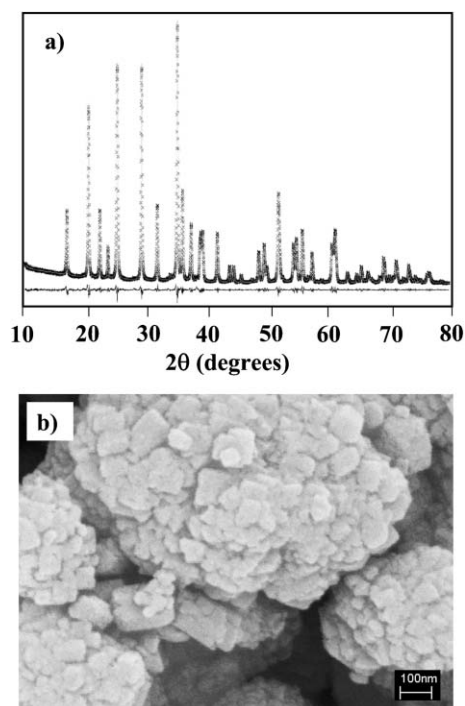
In a separate set of experiments, a mixture of non-ionic surfactants was added to the reactors, including Pluronic P123, FC4, and Jeffamine. The first are block co-polymers of polyethylene oxide and polypropylene oxide, and Jeffamine is a polyoxyalkylamine. Fig. 8b shows an SEM micrograph of a typical sample of LiFePO<sub>4</sub> processed hydrothermally at 220 °C using a mixture of P123 and FC4, followed by firing under Ar at 600 °C. The particle size in this case is smaller and much more homogeneous compared to that of the products using molecular reducing agents, despite the use of the very high autoclave temperature. The particles range in size from 150 nm to about 300 nm. Although the surfactant clearly

**Fig. 8** Raman spectrum (a) and SEM micrograph (b) depicting the effects of non-ionic surfactants (P123 and FC4) on hydrothermal synthesis.

controls crystallite nucleation and growth, like citric acid it does not readily decompose. A Raman spectrum of this product, shown in Fig. 8a, shows a minimum amount of carbon on the surface (0.3 wt% by TGA).

### f) Extension to other LiMPO<sub>4</sub> olivines

Other lithium phospho-olivines including LiMgPO<sub>4</sub> and LiMnPO<sub>4</sub> can also be synthesized hydrothermally using MgSO<sub>4</sub> and MnSO<sub>4</sub>·H<sub>2</sub>O respectively as a substitute for ferrous ammonium sulfate. The lattice parameters for LiMnPO<sub>4</sub> are similar to those reported earlier (Table 1).<sup>31</sup> These compounds can be synthesized with carbon, using the same additives described above. The use of polyacrylic acid also produces nanocrystalline LiMnPO<sub>4</sub>, with particles in the 40–80 nm range (Fig. 9). We were unable to prepare LiNiPO<sub>4</sub> by this method owing to its higher oxidation potential. Note that although nano-triphylite experiences a decrease in unit

**Fig. 9** XRD pattern and LeBail (full pattern matching) refinement (a) and corresponding SEM micrograph (b) of pure LiMnPO<sub>4</sub> synthesized hydrothermally in the presence of polyacrylic acid. The experimental (×) and calculated (—) diffraction patterns are shown, along with the difference curve. Lattice parameters and the agreement factor are given in Table 1.

cell volume, a similar lattice strain on the nano-crystalline LiMnPO<sub>4</sub> seems to have virtually no effect on the lattice parameters. This has also been recently noted in the preparation of a nano-sized divalent manganese compound: MnO.<sup>32</sup> Although line broadening in the diffraction pattern, characteristic of microstrain and small coherence lengths, was observed, little effect on the unit cell volume was noted. The reason for the lattice rigidity of these Mn<sup>2+</sup> materials is unknown. The HDT synthesis can also be extended to form the solid solution series Li(Mg<sub>x</sub>Mn<sub>y</sub>Fe<sub>z</sub>)PO<sub>4</sub>,  $x + y + z = 1$ . Single phase olivine compounds of the solid solution Li(Mn<sub>y</sub>Fe<sub>z</sub>)PO<sub>4</sub>,  $y + z = 1$ , are observed by X-ray diffraction (ESI,† Fig. 1X). These substitutions follow Vegard's law as expected. Solid solution iron/manganese phosphates have been, and are, of particular interest for electrochemical study<sup>10,33</sup> and are currently under investigation.

## Conclusions

While it has previously been shown that hydrothermal synthesis without the presence of reducing or surface active agents does not produce materials with acceptable electrochemistry, our results show that control of temperature and concentration, and the addition of surfactants or polymers, limit particle growth and effectively control the particle size distribution of the particles. Carbon coating the particles can be accomplished with an organic molecule that readily decomposes at low temperature. These modifications to the original hydrothermal process greatly improve the material properties. Further investigations will focus on manipulating the hydrothermal control parameters to obtain nanocrystallites of LiMPO<sub>4</sub> that are <50 Å along the *b*-axis, and which display restricted basal dimensions.

## Acknowledgements

LFN thanks NSERC for funding through the Discovery Grant program and gratefully acknowledges support through the Canada Research Chair award.

## References

- 1 C. S. Cundy and P. A. Cox, *Microporous Mesoporous Mater.*, 2005, **82**, 1.
- 2 G. Armstrong, A. R. Armstrong, J. Canales and P. G. Bruce, *Chem. Commun.*, 2005, 2454.
- 3 A. J. Norquist and D. O'Hare, *J. Am. Chem. Soc.*, 2004, **126**, 6673.

- 4 F. H. Zhao, Q. Su, N. S. Xu, C. R. Ding and M. M. Wu, *J. Mater. Sci.*, 2006, **41**, 1449.
- 5 S. Xiong, B. Xi, W. Wang, C. Wang, L. Fei, H. Zhou and Y. Qian, *Cryst. Growth Des.*, 2006, **6**, 1711.
- 6 L. Zhang, H. Lin, N. Wang, C. Lin and J. Li, *J. Alloys Compd.*, 2007, **431**, 230.
- 7 S. Yang, P. Y. Zavalij and M. S. Whittingham, *Electrochem. Commun.*, 2001, **3**, 505.
- 8 S. Yang, Y. Song, P. Y. Zavalij and M. S. Whittingham, *J. Electrochem. Commun.*, 2002, **4**, 239.
- 9 S. Franger, F. Le Cras, C. Bourbon and H. Rouault, *J. Power Sources*, 2003, **119–121**, 252.
- 10 A. K. Padhi, K. S. Nanjundaswamy and J. B. Goodenough, *J. Electrochem. Soc.*, 1997, **144**, 1188.
- 11 P. S. Herle, B. Ellis, N. Coombs and L. F. Nazar, *Nat. Mater.*, 2004, **3**, 147.
- 12 H. Huang, S.-C. Yin and L. F. Nazar, *Electrochem. Solid-State Lett.*, 2001, **4**, A170.
- 13 R. Dominiko, M. Bele, M. Gaberscek, M. Remskar, S. Pejovnik and J. Jamnik, *J. Electrochem. Soc.*, 2005, **152**, A607.
- 14 A. Yamada, S. C. Chung and K. Hinokuma, *J. Electrochem. Soc.*, 2001, **148**, A224.
- 15 N. Schall, G. Nuspl, V. Christian, L. Wimmer and M. Eisgruber, *Eur. Pat.*, WO2006105848, 2006.
- 16 B. Ellis, W. R. M. Makahnouk and L. F. Nazar, Polymer Battery and Fuel Cell Meeting, PBFC-2, Las Vegas, 2005, Abstract #1.
- 17 J. Chen and M. S. Whittingham, *Electrochem. Commun.*, 2006, **8**, 855.
- 18 B. H. Toby, EXPGUI, a graphical user interface for GSAS, *J. Appl. Crystallogr.*, 2001, **34**, 210–213.
- 19 S. G. Carling, P. Day and D. Visser, *Inorg. Chem.*, 1995, **34**, 3917.
- 20 G. Chen, X. Song and T. J. Richardson, *Electrochem. Solid-State Lett.*, 2006, **9**, A295.
- 21 D. Morgan, A. Van der Ven and G. Ceder, *Electrochem. Solid-State Lett.*, 2004, **7**, A30.
- 22 C. M. Burba and R. Frech, *J. Electrochem. Soc.*, 2004, **151**, A1032.
- 23 F. Croce, A. D'Epifanio, J. Hassoun, A. Deptula, T. Olczac and B. Scrosati, *Electrochem. Solid-State Lett.*, 2002, **5**, A47.
- 24 W. Zhao, Z. Hao and C. Hu, *J. Nanosci. Nanotechnol.*, 2005, **5**, 1752.
- 25 D. Luxembourg, G. Flamant and D. Laplaze, *Carbon*, 2005, **43**, 2302.
- 26 C. Delacourt, P. Poizot, S. Levasseur and C. Masquelier, *Electrochem. Solid-State Lett.*, 2006, **9**, A352.
- 27 J. Barker, M. Y. Saidi and J. L. Swoyer, *Electrochem. Solid-State Lett.*, 2003, **6**, A53.
- 28 J. K. Vassiliou, V. Mehrotra, M. W. Russell, E. P. Giannelis, R. D. McMichael, R. D. Shull and R. F. Ziolo, *J. Appl. Phys.*, 1993, **73**, 5109.
- 29 I. Lopes, N. El Hassan, H. Guerba, G. Wallez and A. Davidson, *Chem. Mater.*, 2006, **18**, 5826.
- 30 S. Tsunekawa, S. Ito and Y. Kawazoe, *Appl. Phys. Lett.*, 2004, **85**, 3845.
- 31 M. Yonemura, A. Yamada, Y. Takei, N. Sonoyama and R. Kanno, *J. Electrochem. Soc.*, 2004, **151**, A1352.
- 32 I. Djerdj, D. Arçon, Z. Jagličić and M. Niederberger, *J. Phys. Chem. C*, 2007, **111**, 3614.
- 33 A. Yamada and S.-C. Chung, *J. Electrochem. Soc.*, 2001, **148**, A960.